Int. J. Electrochem. Sci., 15 **(2020)** 5529 – 5539, doi: 10.20964/2020.06.88

International Journal of
ELECTROCHEMICAL
SCIENCE
www.electrochemsci.org

Short Communication

Preparation of Molybdenum doped Nickel Sulfides Supported on Nickel Foam via Two-step Electrodeposition for Oxygen Evolution Reaction

Yi-Wen Dong, Bao-Yu Guo, Qin-Wei Chen, Bin Dong[*]

College of Science, China University of Petroleum (East China), Qingdao 266580, PR China
[*]E-mail: dongbin@upc.edu.cn

Received: 9 March 2020 / *Accepted:* 14 April 2020 / *Published:* 10 May 2020

Nickel sulfides-based electrocatalyst has been believed to be a very promising alternative for noble metal catalysts for efficient oxygen evolution reaction (OER). However, the dispersion and intrinsic activity of active sites for OER still need improvements. In our work, a facile two-step electrodeposition has been used to help the better dispersion of Ni sties and realize the Mo doping for enhanced intrinsic activity of Ni_3S_2 supported on nickel foam (Mo-Ni_3S_2/NF). Firstly, Mo/Ni/NF as precursor has been obtained by through the two-step electrodeposition of Ni and Mo, respectively. Secondly, the hydrothermal sulfurization of the precursor provides the homogeneous dispersion of Mo-Ni_3S_2 nanoparticles on NF. The prepared Mo-Ni_3S_2/NF for OER only needs a low overpotential of 179 mV to reach the current density of 50 mA cm^{-2} in alkaline solution. The excellent stability has also been kept for more than 10 h. This result suggest that the method of electrodeposition can be a promising way for constructing transition metal-based sulfides electrocatalysts for OER.

Keywords: nickel sulfides; electrodeposition; doping; oxygen evolution reaction

1. INTRODUCTION

With the increasingly serious environmental pollution and energy shortages that hinder the development of the world, green energy has gradually entered people's field of vision [1-10]. Among them, hydrogen molecules have attracted widespread attention due to their high energy density and absolutely clean final product water [11-15]. As a catalyst for the release of hydrogen molecules, precious metal chemical complex Iridium oxides (such as IrO_2) and ruthenium oxides (such as RuO_2) were found be the most active catalysis for oxygen evolution reaction. Nevertheless, due to their expensive price and its low earth content, it cannot be widely applied [16-21]. Therefore, finding effective and cheap catalysts is still a prerequisite for large-scale application of hydrogen energy [22-26].

Based on the earth abundance and chemical properties, molybdenum, nickel are ideal elements of transition metals, which are deemed as potential catalyst for hydrogen evolution reaction (HER), OER, etc [27-30]. However, most materials made by Mo and Ni have been actually prepared for HER. And the reports about OER are very few. For instance, our group has reported a Ni-Co-Mo based catalyst with one-dimensional and hierarchical nanostructures for efficient HER [31]. In addition, The Ni-Mo alloys are helpful for the development of alkaline HER [31]. The major reason lies in the poor catalytic properties of the currently prepared molybdenum and nickel sulfide in the OER reaction [32-36]. Therefore, designing a better Ni-Mo based catalyst for OER is seems meaningful [37].

As for preparation method of catalysts, the most common is one-step synthesis. While saving energy consumption, it also greatly reduces the investment of time. However, due to the uncontrollability of this synthesis method, many active sites cannot be uniformly distributed. And so as to let the performance of the catalyst could not be fully demonstrated. Especially for catalysts containing various metal elements, one-step synthesis method makes it impossible to get directional control between the elements. In order to overcome the problems mentioned above, a stepwise synthesis method is come up.

Herein, a hierarchically structured molybdenum doped nickel sulfide (Mo-Ni_3S_2/NF) has been prepared in a electrodeposition method. And the synthesis process can be divided into three steps, where nickel nanoparticles are first to be electrodeposited on nickel foam (NF); then the molybdenum is electrodeposited onto the surface of nickel nanoparticles; at last, the synthesized molybdenum-nickel precursor is subjected to a brief hydrothermal process, which are all shown in the schematic of Scheme.1. Relevant electrochemical measurements reveal that the obtained Mo-Ni_3S_2/NF has an excellent catalytic ability for OER and only requires a low overpotential of 179 mV to reach the current density of 50 mA cm^{-2}, which can rivaling the most reported transition metal based catalysts at large current density (Table 1). This work may provide an idea for the synthesis of Mo-Ni-based catalysts, so that they can be applied for other based OER progress.

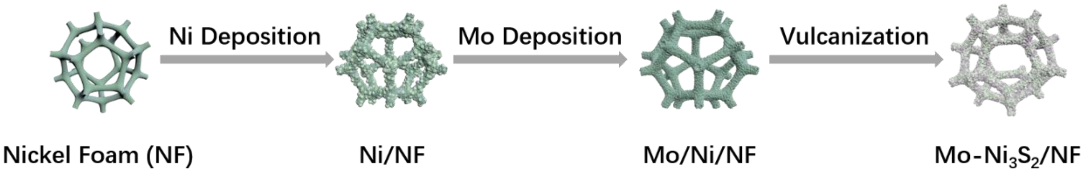

Scheme. 1 Schematic diagram of Mo-Ni_3S_2/NF synthesis.

2. EXPERIMENTAL SECTION

2.1 Synthesis of the Ni/NF

One piece of clean nickel foam (1×2 cm^2), the saturated calomel electrode and a graphite rod serve as the working electrode, reference electrode and counter electrode, respectively. And then electrodeposition operation is performed at -0.85 V for 20 mins in the bath solution, which contains 0.1 M Nickel sulfate hexahydrate ($NiSO_4{\cdot}6H_2O$), 0.5 M boracic acid (H_3BO_3) and 30 ml water. After that, the prepared specimen is rinsed three times with ethanol and deionized water before vacuum drying.

2.2 Synthesis of the Mo/Ni/NF

The precursor obtained in the previous step is immerged in 20 ml 0.2 M Sodium molybdate dihydrate ($Na_2MO_4{\cdot}H_2O$) homogenous solution for 4 hours, which then serves as working electrode. Nickel foam and saturated calomel electrode (SCE) are used as the counter electrode, and then the precursor is electrodeposited in 20 ml 0.2 M sodium molybdate solution. Finally, the sample is cleaned by deionized water and ethanol for three times before vacuum drying.

2.3 Synthesis of the Mo-Ni_3S_2/NF

The sample obtained above is hydrothermally reacted in a 30 ml solution configured by 0.15 g of thioacetamide and 0.0591 g of glutathione at 140 ℃ for 12 hours. Then the obtained product is washed several times with deionized water and ethanol.

2.4 Material characterization

The microscopic morphology of the sample is indicated by obtaining Scanning electron microscopy (SEM) images (Hitachi S-4800). The X-ray diffraction(XRD) data are recorded on the X'Pert PRO MPO diffractometer utilizing Cu Kα with 2θ range from 5° to 75°. X-ray photoelectron spectroscopy (XPS) is performed on a Thermo Fisher Scientific II spectrometer utilizing Al as the photo-source.

2.5 Electrochemical measurements

The electrochemical properties of all samples are measured on a typical device (Gamry 3000) in 1.0 M KOH electrolytic solution (where pH = 14). The method utilizes the preliminary sample as the working electrode, the saturated calomel electrode (SCE) as the reference electrode and the a graphite rod as the counter electrode. The potential conversion from E (SCE) to the reversible hydrogen electrode (RHE) is based on the following equation: E (RHE) = E (SCE) + 0.243 + 0.059 pH. The linear sweep voltammetry (LSV) test for OER are measured at a scan rate of 5 mV s^{-1}. Cyclic voltammograms (CV) are acquired at scanning speed of 40, 60, 80, 100, and 120 mV s^{-1}. In addition, the samples' stabilities are obtained by a chronoamperometry program. And the electrochemical impedance spectroscopy (EIS) measurements were tested at an invariable potential in frequency from 10^{-2} to 10^5 Hz.

3. RESULTS AND DISCUSSION

The structure of the as-prepared samples has been characterized by XRD (Fig. 1a). As shown, three are three diffraction peaks at 44.4°, 51.8° and 76.3° that involved in Ni/NF and Mo/Ni/NF, which is corresponding to the facets of (111), (200) and (220) for nickel foam (PDF no.01-070-1849). After the final vulcanization step, the obtained Mo-Ni_3S_2/NF (Fig. 1b) has five other peaks, which contains 21.7°, 31.0°, 37.7°, 49.7°, and 55.2°, respectively. Corresponding to the lattice of Ni_3S_2 (PDF No. 01-076-1870) [38-39]. Besides, the peaks are narrow, reflecting its high crystalline structure. Nevertheless, there are no peaks that represent MoS in the diffraction pattern of the final vulcanization product, indicating an amorphous structure of Mo element.

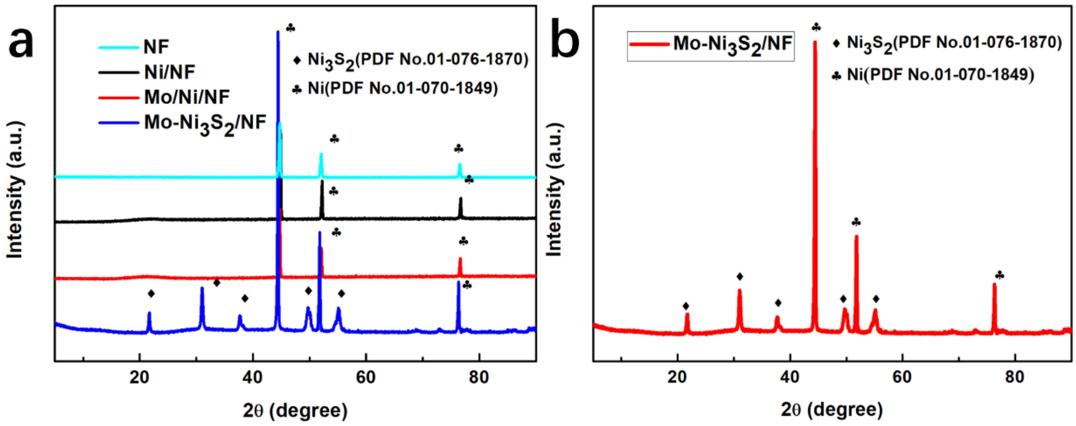

Figure 1. (a) XRD patterns of NF, Ni/NF, Mo/Ni/NF and Mo-Ni_3S_2/NF samples; (b) XRD pattern of Mo-Ni_3S_2/NF.

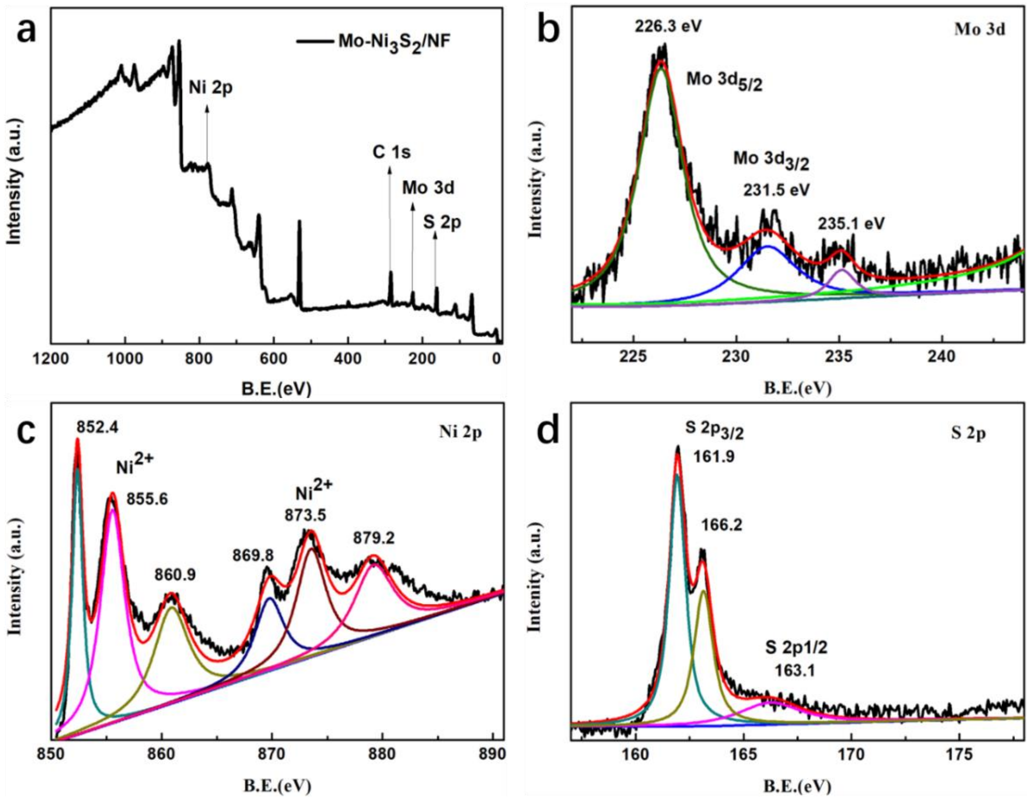

Figure 2. XPS spectra of Mo-Ni_3S_2/NF sample. (a) survey; (b) Mo 3d; (c) Ni 2p and (d) S 2p.

In order to confirm the chemical composition and electronic state of Mo-Ni_3S_2/NF, X-ray photoelectron spectroscopy (XPS) test is conducted. Fig. 2a is the results of Mo-Ni_3S_2/NF survey, which has the elements of Mo, Ni, S and C. In Fig. 2c, the Ni 2p spectrum shows six peaks. Two peaks at 852.4 and 869.8 eV, which are corresponding to NiS and the peaks at 855.6 and 873.5 eV is for oxidic Ni^{2+} region [39]. The other peaks at 860.9 and 879.2 eV binding energies are satellite peaks (Sat.) of nickel. In the Mo 3d spectrum (Fig. 2b), the binding energy of 226.3 and 231.5 eV are attributed to Mo $3d_{5/2}$ and Mo $3d_{3/2}$, and the peak of 231.5 eV give an index to +6 oxidation state of Mo ion. Besides, the peaks at 235.1 eV is the satellite peak (Sat.) of molybdenum [40]. In addition, as for S 2p spectrum (Fig. 2d), two spin-orbit doublet peaks at 161.9 and 163.1 eV are observed, which can be indexed to S $2p_{3/2}$ and S $2p_{1/2}$, respectively [39].

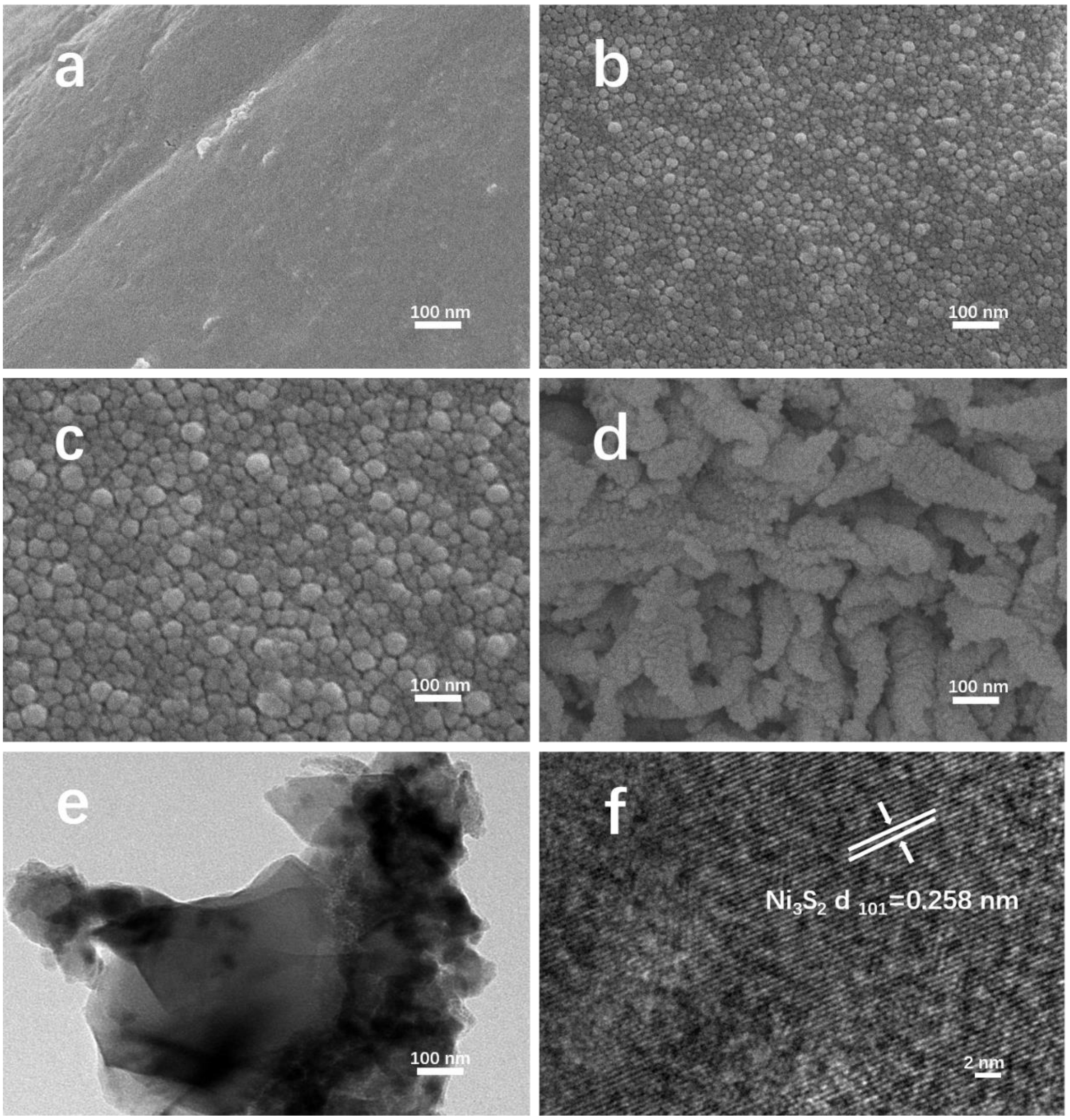

Figure 3. (a) SEM image of NF; (b) SEM image of Ni/NF; (c) SEM image of Mo/Ni/NF; (d) SEM image of Mo-Ni_3S_2/NF and (e, f) HRTEM images of Mo-Ni_3S_2/NF.

The microscopic surface morphologies of the specimen are explored by SEM in the Fig. 3. As for the clean nickel foam (Fig. 3a), the surface is smooth, which is providing the substrate for the deposition of Ni and Mo. After the electrodeposition of nickel, the surface of the NF is coverd with nanospheres, ranging from 20 nm to 30 nm (Fig. 3b), that is formed by Ni substance. Besides, the molybdenum deposition makes nanospheres grow bigger to 40 nm to 50 nm that is shown in Fig. 3c. After the vulcanization processing, the nanoparticals aggregate into irregular morphology with the size of 200 nm to 300 nm (Fig. 3d). On the surface of them, there are many fine wrinkles, which can provide more surface area for generating more active sites. Besides, the high-resolution transmission electron microscopy (HRTEM) image (Fig. 3e-f) reveals that distinct lattice streaks with interplane distance of 0.258 nm, which corresponds to the (101) plane of Ni_3S_2, which also proves the amorphous state of molybdenum.

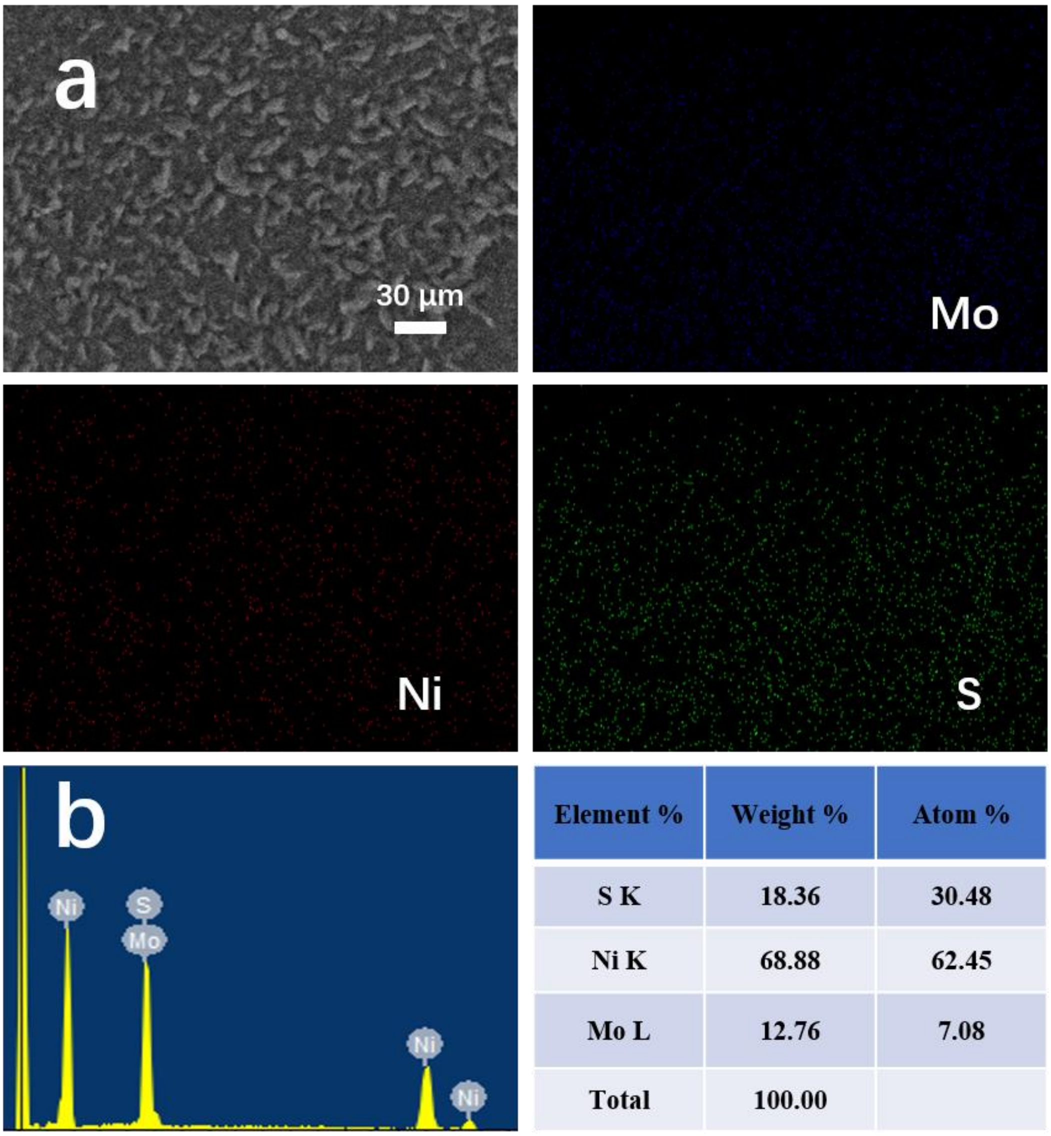

Element %	Weight %	Atom %
S K	18.36	30.48
Ni K	68.88	62.45
Mo L	12.76	7.08
Total	100.00	

Figure 4. (a) SEM mapping of Mo-Ni_3S_2/NF, (b) EDX of Mo-Ni_3S_2/NF.

In order to know the surface element distribution, a SEM mapping analysis has been performed (Fig. 4a), and the results confirms that the elements containing Mo, Ni, and S are evenly distributed on the Mo-Ni_3S_2/NF catalyst. Moreover, Energy Dispersive X-ray (EDX) is employed to analyze the element distribution. As is shown in Fig. 4b, the elemental molar concentrations of Mo, Ni and S in Mo-Ni_3S_2/NF are 12.76 %, 68.88 % and 18.36 %.

Meanwhile, the electrochemical properties of Ni/NF, Mo/Ni/NF and Mo-Ni_3S_2/NF are measured in 1.0 M KOH solution. From the OER polarization curve (Fig. 5a), catalytic capacity of each sample is demonstrated. Ni/NF and Mo/Ni/NF performs general nature, which require an overpotential of 500 mV and 537mV to transfer a current density of 50 mA cm^{-2}, respectively. However, sulfide products Mo-Ni_3S_2/NF exhibits enhanced catalytic capacity with an overpotential of 179 mV at 50 mA cm^{-2} current density, performing better than other reported similar catalysts. Besides, in order to affirm the effect of Mo doping, NiS/NF is also tested, the results show that its overpotential is 400 mV that is larger than Mo-Ni_3S_2/NF, which mirrors the significate role of Mo doping. At the same time, the Tafel slopes of each sample (Fig. 5b) are explored to know the reaction kinetics. As shown, the Tafel slope of Mo-Ni_3S_2/NF (60 mV dec^{-1}) is lower than those of other comparisons, which contain NiS/NF (140 mV dec^{-1}), Ni/NF (109 mV dec^{-1}) and Mo/Ni/NF (104 mV dec^{-1}) electrodes, proving a faster reaction rate.

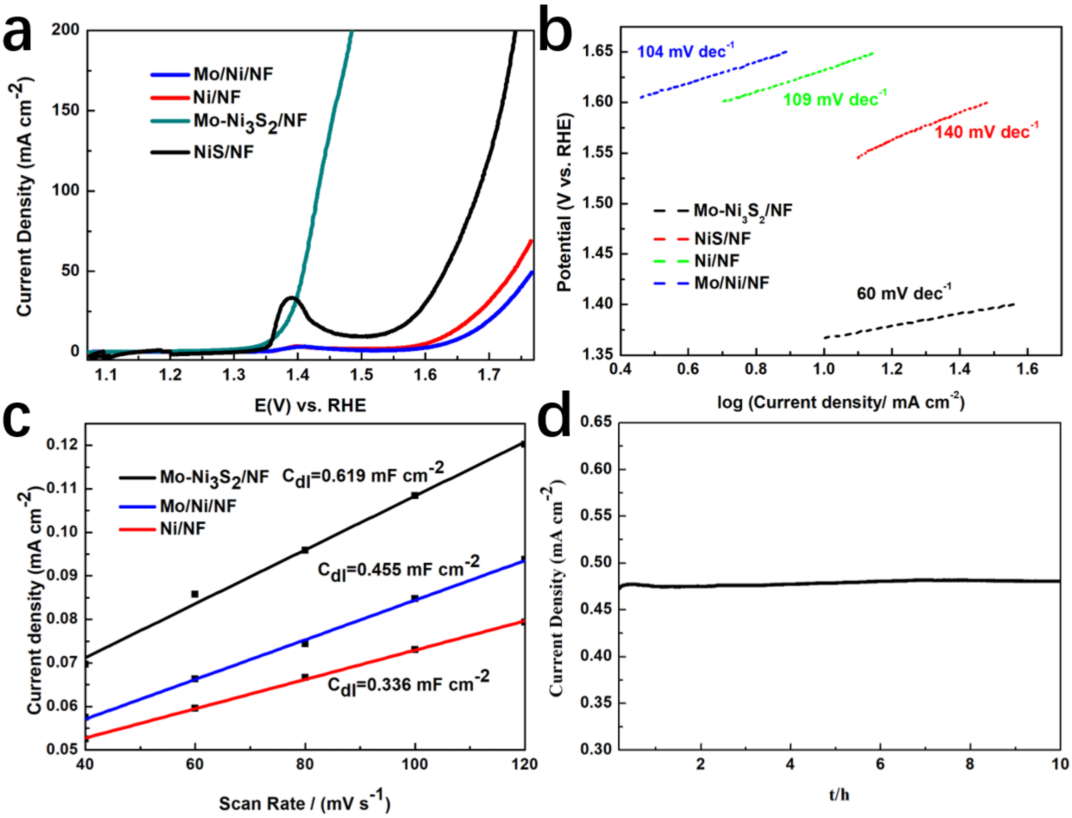

Figure 5. (a) LSV curves of each sample after OER process in 1 M KOH, (b) Tafel plots of Mo-Ni_3S_2/NF, NiS/NF, Ni/NF and Mo/Ni/NF; (c) Double-layer capacitance for Ni/NF, Mo/Ni/NF and Mo-Ni_3S_2/NF/NF samples in 1 M KOH: relationship between scan rate and current density; (d) stability test of Mo-Ni_3S_2/NF (I-T for 10 hour).

Table 1 Comparison of OER performance between Mo-Ni_3S_2/NF and other non-precious metal catalyst

Electrocatalyst	**Electrolyte**	**Overpotential at 50 mA cm^{-2} (mV)**	**Reference**
Mo-Ni_3S_2/NF	**1 M KOH**	**179**	**This work**
NiS-MoS_2	1 M KOH	300	41
MoS_2 on Ni foam	1 M KOH	430	42
$Mo_{5.9}Ni_{94.1}S$/NF	1 M KOH	350	43
Mo-doped Ni_3S_2	1 M KOH	180	44
Mo doped NiS/Ti	1 M KOH	390	45
Fe-MoS_2	1 M KOH	290	46
N-$(Ni,Fe)_3S_2$/NIF	1 M KOH	195	47
$(BO_3)_{1.08}$-Ni_3S_4	1 M KOH	330	48
$Ni_{0.9}Fe_{0.1}MoO_4$	1 M KOH	380	49
MoCoNiS/NF	1 M KOH	204	50

The electrochemical active surface area (ECSA) of Ni/NF, Mo/Ni/NF and Mo-Ni_3S_2/NF samples are also measured to compare the effective catalytic area by comparing the electrochemical double-layer capacitance (C_{dl}), which is in direct proportion to ECSA and surface roughness. Fig.5c shows the value of Ni/NF is 0.336 mF cm^{-2}, the Mo/Ni/NF is 0.455 mF cm^{-2} and the Mo-Ni_3S_2/NF is 0.619 mF cm^{-2}, respectively. From the above discussion, it is known that the improvement in catalytic performance is partly attributed to the larger ECSA. Moreover, to ascertain the electrochemical stability of the Mo-Ni_3S_2/NF, a chronoamperometry test is experimentally operated (Fig. 5d). The current-time curve reflects 10-hour steady current, which means that Mo-Ni_3S_2/NF can keep high activity during actual catalysis experiments for a long time.

4. CONLUSIONS

In summary, a two-step electrodeposition route has been designed to synthesize the Mo-Ni_3S_2/NF, which shows excellent catalytic performance in the alkaline OER process. Where the transition metal Mo and Ni are used innovatively to catalyze OER course rather than HER. In actual catalysis experiments, the final-product Mo-Ni_3S_2/NF performs well with a lower overpotential (179 mV to reach the current density of 50 mA cm^{-2}), smaller Tafel slope (60 mV dec^{-1}) and larger C_{dl} value (0.619 mF cm^{-2}). At the same time, it can maintain a long-time stability for more than ten hours. This work may provide an idea for step-by-step synthesis of catalysis and make them more widely used in the field of electrocatalysis.

ACKNOWLEDGEMENTS
This work is financially supported by Shandong Provincial Natural Science Foundation (ZR2017MB059).

Reference

1. X. L. Tian, X. Zhao, Y. Q. Su, L. J. Wang, H. M. Wang, D. Dang, B. Chi, H. F. Liu, E. J. M. Hensen, X. W. Lou, B. Y. Xia, *Science*, 366 (2019) 850.
2. X. Shang, W. H. Hu, X. Li, B. Dong, Y. R. Liu, G. Q. Han, Y. M. Chai, C. G. Liu, *Electrochim. Acta*, 224 (2017) 25.
3. T. Wu, S. Sun, J. Song, S. Xi, Y. Du, B. Chen, W. A. Sasangka, H. Liao, C. L. Gan, G.G. Scherer, L. Zeng, H. Wang, H. Li, A. Grimaud, Z. J. Xu, *Nat. Catal.*, 2 (2019) 763.
4. X. Chia, M. Pumera, *Nat. Catal.*, 1 (2018) 909.
5. X. Wang, A. Vasileff, Y. Jiao, Y. Zheng, S.Z. Qiao, *Adv. Mater.*, 30 (2018) 1803625.
6. Q. Hu, G. Li, X. Liu, B. Zhu, X. Chai, Q. Zhang, J. Liu, C. He, *Angew. Chem. Int. Ed.*, 58 (2019) 4318.
7. Q. Hu, X. Liu, B. Zhu, L. Fan, X. Chai, Q. Zhang, J. Liu, C. He, Z. Lin, *Nano Energy,* 50 (2018) 212.
8. X. Shang, K.L. Yan, Y. Rao, B. Dong, J.Q. Chi, Y.R. Liu, X. Li, Y.M. Chai, C.G. Liu, *Nanoscale*, 9 (2017) 12353.
9. D. Zhang, H. Zhao, B. Huang, B. Li, H. Li, Y. Han, Z. Wang, X. Wu, Y. Pan, Y. Sun, X. Sun, J. Lai, L. Wang, *ACS Cent. Sci.*, 5 (2019) 1991.
10. B.Q. Li, C.X. Zhao, S. Chen, J.N. Liu, X. Chen, L. Song, Q. Zhang, *Adv. Mater.*, 31 (2019) 1900592.
11. F. Guo, Y. Wu, H. Chen, Y. Liu, L. Yang, X. Ai, X. Zou, *Energy Environ. Sci.*, 12 (2019) 684.
12. Y.M. Du, M.J. Zhang, Z.C. Wang, Y.R. Liu, Y.J. Liu, Y.L. Geng, L. Wang, *J. Mater. Chem. A.*, 7 (2019) 8602.
13. W.H. Hu, R. Yu, G.Q. Han, Y.R. Liu, B. Dong, Y.M. Chai, Y.Q. Liu, C.G. Liu, *Mater. Lett.*, 161 (2015) 120.
14. Z. J. Xu, *Nano-Micro Lett.*, 10 (2018) 8.
15. H. Chen, X. Ai, W. Liu, Z. Xie, W. Feng, W. Chen, X. Zou, *Angew. Chem. Int. Ed.*, 58 (2019) 11409.
16. Y. Yu, Y. Shi, B. Zhang, *Acc. Chem. Res.*, 51 (2018) 1711.
17. G.Q. Han, Y.R. Liu, W.H. Hu, B. Dong, X. Li, Y.M. Chai, Y.Q. Liu, C.G. Liu, *Materials Chemistry*

and Physics, 167 (2015) 271.
18. A. Li, Y. Sun, T. Yao, H. Han, *Chemistry-A European Journal*, 24 (2018) (69) 18334.
19. B.Y. Guo, X.Y. Zhang, X. Ma, T.S. Chen, M.L. Wen, X.L. Yang, J.F. Qin, Y.M. Chai, J. Nan, B. Dong, *Inter. J. Hydrogen Energy,* 45 (2020) 9575.
20. J. Zhang, X. Shang, H. Ren, J. Chi, H. Fu, B. Dong, C. Liu, Y. Chai, *Adv. Mater.*, 31 (2019) 1905107.
21. T. Liu, P. Li, N. Yao, G. Cheng, S. Chen, W. Luo, Y. Yin, *Angew. Chem. Int. Ed.*, 58 (2019) 4976.
22. K.L. Yan, J.Q. Chi, J.Y. Xie, B. Dong, Z.Z. Liu, W.K. Gao, J.H. Lin, Y.M. Chai, C.G. Liu, *Renewable Energy*, 119 (2018) 54.
23. L.J. Yang, Y.Q. Deng, X.F. Zhang, H. Liu, W.J. Zhou, *Nanoscale*, 10 (2018) 9268.
24. Y.R. Liu, W.H. Hu, G.Q. Han, B. Dong, X. Li, X. Shang, Y.M. Chai, Y.Q. Liu, C.G. Liu, *Electrochimica Acta*, 220 (2016) 98.
25. Y. Zhao, X. Zhang, X. Jia, G.I.N. Waterhouse, R. Shi, X. Zhang, F. Zhan, Y. Tao, L.Z. Wu, C.H. Tung, D. O'Hare, T. Zhang, *Adv. Energy Mater.*, 8 (2018) 1703585.
26. S. Sun, Y. Sun, Y. Zhou, S. Xi, X. Ren, B. Huang, H. Liao, L. P. Wang, Y. Du, Z. J. Xu, *Angew. Chem. Int. Ed.*, 58 (2019) 6042.
27. Y. Chen, H. Li, J. Wang, Y. Du, S. Xi, Y. Sun, M. Sherburne, J.W. Ager III, A. C. Fisher, Z. J. Xu, *Nat. Commun.*, 10 (2019) 572.
28. C. Lei, W. Zhou, Q. Feng, Y. Lei, Y. Zhang, Y. Chen, J. Qin, *Nano-Micro Lett.*, 11 (2019) 45.
29. W.H. Hu, X. Shang, J. Xue, B. Dong, J.Q. Chi, G.Q. Han, Y.R. Liu, X. Li, K.L. Yan, Y.M. Chai, C.G. Liu, *Int. J. Hydrogen Energy*, 42 (2017) 2088.
30. S. Deng, K. Zhang, D. Xie, Y. Zhang, Y. Zhang, Y. Wang, J. Wu, X. Wang, H.J. Fan, X. Xia, J. Tu, *Nano-Micro Lett.*, 11 (2019) 12.
31. Z.Z. Liu, X. Shang, B. Dong, Y.M. Chai, *J. Catalysis*, 361 (2018) 204.
32. X. Zhao, J. Meng, Z. Yan, F. Cheng, J. Cheng, *Chinese Chemical Letters*, 30 (2019) 319.
33. B. Liu, X.Y. Zhang, T.S. Chen, L.M. Zhang, X.L. Yang, X. Ma, D. Liu, *Int. J. Electrochem. Sci.*, 13 (2018) 8506.
34. M.A.R. Anjum, J.S. Lee, *ACS Catalysis*, 7 (2017) 3030.
35. H.X. Ang, H.T. Tan, Z.M. Luo, Y. Zhang, Y.Y. Guo, G.L. Guo, H. Zhang, Q.Y. Yan, *Small*, 11 (2015) 6278.
36. G.Q. Han, X. Li, J. Xue, B. Dong, X. Shang, W.H. Hu, Y.R. Liu, J.Q. Chi, K.L. Yan, Y.M. Chai, C.G. Liu, *Int. J. Hydrogen Energy*, 42 (2017) 2952.
37. L. An, J. Feng, Y. Zhang, R. Wang, H. Liu, H. Liu, G.C. Wang, F. Cheng, P. Xi, *Adv. Funct. Mater.*, 29 (2019) 1805298.
38. Z. Cui, Y.C. Ge, H. Chu, R. Baines, P. Dong, J.H. Tang, Y. Yang, P.M. Ajayan, M.X. Ye, J.F. Shen, *J. Mater. Chem. A*, 5 (2017) 1595.
39. K. Jayaramulu, J. Masa, O. Tomanec, D. Peeters, V. Ranc, A. Schneemann, R. Zboril, W. Schuhmann, R.A. Fischer, *Adv. Funct. Mater.*, 27 (2017) 1700451.
40. C. Xie, Y.Y. Wang, K. Hu, L. Tao, X.B. Huang, J. Huo, S.Y. Wang, *J. Mater. Chem. A*, 5 (2017) 87.
41. S.D. Guan, X.L. Fu, Z.Z. Lao, C.H. Jin, Z.J. Peng, *Sustainable Energy & Fuels*, 3 (2019) 2056.
42. K. Yan, Y.R. Lu, *Small*, 12 (2016) 2975.
43. C. Du, Y.N. Men, X.Z. Hei, J.H. Yu, G.Z. Cheng, W. Luo, *ChemElectroChem*, 5 (2018) 2564.
44. Z. Cui, Y.C. Ge, H. Chu, R. Baines, P. Dong, J.H. Tang, Y. Yang, P.M. Ajayan, M.X. Ye, J.F. Shen, *Journal of Materials Chemistry A*, 5 (2017) 1595.
45. Q. Jia, X.X. Wang, S. Wei, C.L. Zhou, J.M. Wang, J.Q. Liu, *Applied Surface Science*, 484 (2019) 1052.
46. B.S. Tang, Z.G. Yu, H.L. Seng, N.D. Zhang, X.X. Liu, Y.W. Zhang, W.F. Yang, H. Gong, *Nanoscale*, 10 (2018) 20113.
47. Y. S. Jin, X. Yue, H.Y. Du, K. Wang, S.L. Huang, P.K. Shen, *Journal of Materials Chemistry A*, 6 (2018) 5592.

48. Z. Zhang, T.R. Zhang, J.Y. Lee, *ChemElectroChem*, 6 (2019) 1443.
49. J.Y. Chen, G.Q. Zhao, Y.P. Chen, K. Rui, H. Mao, S.X. Dou, W.P. Sun, *Chemistry–A European Journal*, 25 (2019) 280.
50. J.F. Qin, M. Yang, T.S. Chen, B. Dong, S. Hou, X. Ma, Y.N. Zhou, X.L. Yang, J, Nan, Y.M. Chai, *International Journal of Hydrogen Energy*, 45 (2020) 2745.